Proc. Natl. Acad. Sci. USA
Vol. 93, pp. 7008–7012, July 1996
Biophysics

Structure of the ripple phase in lecithin bilayers

(biomembranes/phospholipids/x-ray diffraction)

W.-J. SUN†, S. TRISTRAM-NAGLE‡, R. M. SUTER†, AND J. F. NAGLE*†‡§

Departments of †Physics and ‡Biological Sciences, Carnegie Mellon University, Pittsburgh, PA 15213

Communicated by Watt W. Webb, Cornell University, Ithaca, NY, April 9, 1996 (received for review December 27, 1995)

ABSTRACT **The phases of the x-ray form factors are derived for the ripple ($P_{\beta'}$) thermodynamic phase in the lecithin bilayer system. By combining these phases with experimental intensity data, the electron density map of the ripple phase of dimyristoyl-phosphatidylcholine is constructed. The phases are derived by fitting the intensity data to two-dimensional electron density models, which are created by convolving an asymmetric triangular ripple profile with a transbilayer electron density profile. The robustness of the model method is indicated by the result that many different models of the transbilayer profile yield essentially the same phases, except for the weaker, purely ripple (0,k) peaks. Even with this residual ambiguity, the ripple profile is well determined, resulting in 19 Å for the ripple amplitude and 10° and 26° for the slopes of the major and the minor sides, respectively. Estimates for the bilayer head–head spacings show that the major side of the ripple is consistent with gel-like structure, and the minor side appears to be thinner with lower electron density.**

Lipids in water self-assemble into lamellar bilayers, which comprise the basic structural element of biomembranes. The supramolecular packing of the bilayers, in turn, forms lyotropic liquid crystals with rich phase behavior and diverse structures. Among the thermodynamic phases observed in lipid bilayer systems, the ripple ($P_{\beta'}$) phase in lecithin bilayers is especially fascinating to a broad range of researchers in condensed matter physics and physical chemistry as an example of periodically modulated phases. Many theoretical papers have attempted to explain the formation of the ripples (1–8). Such understanding has been delayed because, despite many experimental studies (9–19), the structure has not been as well characterized as have the structures for the lower temperature gel ($L_{\beta'}$) phase (20) and the higher temperature liquid crystalline (L_α) phase (21). When an accurate ripple structure is known, some indication of the energetics of the ripple formation may be obtained by comparing the relative size of the ripple wavelength and the ripple amplitude to the size of lipid molecules and the bilayer thickness (5). Also, correlation between the chirality of the constituent lipid molecules and the asymmetry of the ripples may lead to elucidation of the microscopic origin of the macroscopic properties of the ripple phase (8, 19).

Structural information about the ripple phase can be divided into two categories. The first category consists of the two-dimensional lattice parameters, namely, the ripple wavelength λ_r, the bilayer packing repeat distance d, and the oblique angle γ for the unit cell that are illustrated in Fig. 1. These well-established parameters have been accurately obtained by indexing low-angle x-ray scattering peaks (9, 10, 12, 16, 18). For example, Wack and Webb (18) reported for dimyristoyl-phosphatidylcholine (DMPC) with 25% water by weight at 18°C that λ_r = 141.7 Å, d = 57.94 Å, and γ = 98.4°. The second category consists of the structure within the ripple unit cell, including the shape and the amplitude of the ripples and the bilayer thickness. This second category of structural information has been quite uncertain. Many ripple profiles have been proposed (1, 2, 4–10, 14), including sinusoidal, peristaltic, and sawtooth and estimates of the ripple trough-to-peak amplitude range widely from 15 to 50 Å (9, 10, 14, 22, 23).

The second category of information involves electron density maps. These require the amplitudes of the form factors, which, ignoring fluctuation corrections (21), are the square roots of the Lorentz-corrected intensities of the x-ray scattering peaks, and the correct phases for these measured form factor amplitudes. A traditional approach to solve the phase problem is the "pattern recognition" method employed by Tardieu and coworkers (9); this method selects those phase combinations that will give rise to electron density maps agreeing with known physical properties of the bilayer system. Considering that there are typically 20 or so peaks in most of the ripple phase x-ray data, finding the right phase combination out of about 2^{20} possibilities is a difficult task. The approach we employed involved modeling and nonlinear least squares fitting. Possibly, this method may be generally useful when studying other disordered and fluctuating biological systems that have intrinsically continuous electron density maps rather than an atomic resolution crystal structure.

METHODS

The modeling approach first creates a functional form for the electron density that incorporates known and plausible properties of the bilayer but that contains free parameters to incorporate unknown detailed structure. The success of the method depends on this modelling step, which requires some care and is, therefore, the emphasis of this section. Then, the values of the free parameters in the real space model are determined by routine nonlinear least squares procedures so that the Fourier components of the model provide the best fit to the measured intensities. This last step automatically determines the phases of the model, which are then used with the original intensity data to produce an electron density map.

Lattice Structure. It has been shown from x-ray studies (9, 10, 12, 16, 18, 19) that ripples in different bilayers are registered to form a two-dimensional oblique lattice as shown by the unit cell in Fig. 1. The unit cell vectors can be expressed (see Fig. 1) as

$$\vec{a} = d \cot\gamma\, \hat{x} + d\, \hat{z} \text{ and } \vec{b} = \lambda_r\, \hat{x}. \qquad [1]$$

The corresponding reciprocal lattice unit cell vectors (see Fig. 1) are

$$\vec{A} = \frac{2\pi}{d}\hat{z} \text{ and } \vec{B} = \frac{2\pi}{\lambda_r}\hat{x} - \frac{2\pi}{\lambda_r \tan\gamma}\hat{z}, \qquad [2]$$

The publication costs of this article were defrayed in part by page charge payment. This article must therefore be hereby marked "*advertisement*" in accordance with 18 U.S.C. §1734 solely to indicate this fact.

Abbreviations: DMPC, dimyristoyl-phosphatidylcholine; SDF, simple delta function; MDF, modulated delta function; M1G, modulated 1G.

§To whom reprint requests should be addressed.

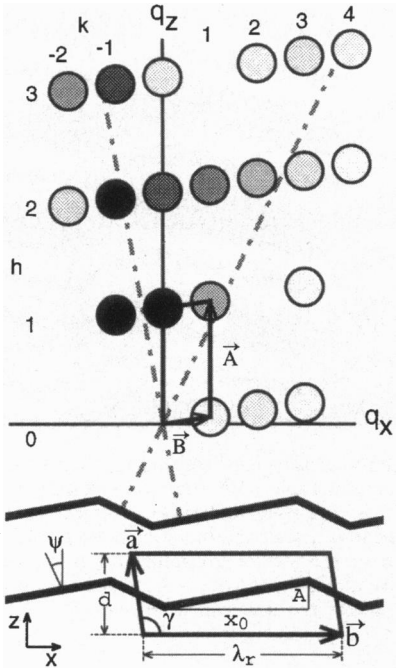

FIG. 1. Real space pattern (*Lower*) shows the asymmetric ripple profile by bold lines for two bilayers. The q-space pattern (*Upper*) shows the (h,k) peak positions as the centers of the circles. Larger magnitudes of the form factors for reflections that were observed (18) are indicated by darker circles. The dot-dash lines show the perpendiculars to the major and the minor sides of the ripple profile.

so the q-space vector $\vec{q}_{hk}$ for the Bragg peak with Miller indices (h,k) is

$$\vec{q}_{hk} = h\vec{A} + k\vec{B}, \qquad [3]$$

with some examples shown in Fig. 1.

Electron Density Model and Form Factor. The ripple profile is the line $z = u(x)$ that describes the center of the bilayer in the (x,z) plane, such as the one shown in Fig. 1. The closely related contour function is defined as

$$C(x,z) = \delta[z - u(x)]. \qquad [4]$$

The transbilayer electron density function $T_\psi(x,z)$ expresses the actual electron density at points (x,z) that lie on a straight line with slope ψ from the vertical as shown in Fig. 1. An underlying electron density profile will be chosen similar to models for flat bilayer phases. Then, the electron density model for $\rho(x,z)$ within the unit cell is described as the convolution of a ripple contour function $C(x,z)$ and the transbilayer electron density profile $T_\psi(x,z)$:

$$\rho(x,z) = C(x,z) * T_\psi(x,z). \qquad [5]$$

This convolution moves the transbilayer electron density function so that it is centered on the ripple profile.

The form factor $F(\vec{q})$ is the Fourier transform of the electron density expressed in Eq. **5** and is the product

$$F(\vec{q}) = F_C(\vec{q})F_T(\vec{q}) \qquad [6]$$

of the Fourier transform $F_C(q)$ of $C(x,z)$ and of the Fourier transform $F_T(q)$ of $T_\psi(x,z)$.

Ripple Profile. The results of freeze fracture electron microscopy (11, 13, 15) and scanning tunneling microscopy (22, 23) strongly suggest that the ripple profile is asymmetric. This conclusion is further supported by the result of x-ray diffraction, in which the ripple unit cell is oblique (γ not equal to 90°) (9, 10, 12, 16–19). For our model ripple profile $u(x)$, we choose a triangular shape as shown in Fig. 1. We shall call the longer side of the ripple the major side, and the shorter side the minor side. The triangular ripple profile is completely described by the amplitude A and x_0, the projection of the major side onto the x axis, with obvious relations for other quantities such as the slope angles of the major and minor sides. Choosing the origin at the center of the unit cell shown in Fig. 1 gives the ripple profile

$$u(x) = \begin{cases} -\dfrac{A}{\lambda_r - x_0}\left(x + \dfrac{\lambda_r}{2}\right) & \text{if } -\dfrac{\lambda_r}{2} \le x < -\dfrac{x_0}{2}; \\ \dfrac{A}{x_0}x & \text{if } -\dfrac{x_0}{2} \le x \le \dfrac{x_0}{2}; \\ -\dfrac{A}{\lambda_r - x_0}\left(x - \dfrac{\lambda_r}{2}\right) & \text{if } \dfrac{x_0}{2} < x \le \dfrac{\lambda_r}{2}. \end{cases} \qquad [7]$$

This particular choice shows explicitly the inversion symmetry in the ripple profile, so that the form factors are real.

Using Eq. **7**, the contour part of the form factor is

$$F_C(\vec{q}) = \frac{1}{\lambda_r}\int_{-\frac{\lambda_r}{2}}^{\frac{\lambda_r}{2}} dx\, e^{i[q_x x + q_z u(x)]}$$

$$= \frac{x_0}{\lambda_r}\,\mathrm{sinc}(\omega) + \frac{\lambda_r - x_0}{\lambda_r}\,\frac{\cos\frac{1}{2}\left(\frac{1}{2}q_x\lambda_r + \omega\right)}{\cos\frac{1}{2}\left(\frac{1}{2}q_x\lambda_r - \omega\right)}$$

$$\times\ \mathrm{sinc}\left(\frac{q_x\lambda_r}{2} - \omega\right), \qquad [8]$$

where the intermediate variable ω is defined as

$$\omega(\vec{q}) = \frac{1}{2}(q_x x_0 + q_z A). \qquad [9]$$

The first term on the right hand side of Eq. **8** is the contribution from the major side of the ripple, with scattering amplitude x_0/λ_r, proportional to its projected length onto the x axis, whereas the last term is the contribution from the minor side of the ripple, with amplitude $(\lambda - x_0)/\lambda_r$. Eq. **8** also shows that the maximum scattering from the major side occurs along that $\vec{q}$ direction determined by $\omega = 0$ in Eq. **9**. In real space, this is also the direction normal to the major side of the ripple. Similarly, the maximum scattering direction of the minor side is given by $q_x\lambda_r/2 - \omega = 0$, and this can be shown to be the direction normal to the minor side. These directions are illustrated by the dot-dashed lines in Fig. 1. This theoretical picture for the location of the strong (h,k) peaks agrees qualitatively with the experimental intensity pattern of Wack and Webb (18) shown in Fig. 1 as well as other x-ray data (16, 19). This general pattern would also be expected to pertain to ripple profiles that are not perfectly triangular, for example, with rounded corners.

Transbilayer Electron Density Profile $T_\psi(x,z)$. In a study of gel phase DPPC bilayers using the electron density modeling approach (24), it was found that the precise functional form of the electron density model did not much affect the results provided that the essential structural features of bilayers were incorporated into the model. Therefore, we first used a very simple model for $T_\psi(x,z)$ in which the two opposite headgroup regions consist of two identical positive δ functions, with amplitude ρ_H, separated by the head–head spacing $2X_h$, and with the central methyl trough consisting of a negative δ function, with amplitude ρ_M. The methylene region of bilayers has an electron density close to that of water and hence is set

equal to zero in the following model [minus fluid (25)] of $T_\psi(x,z)$:

$$T_\psi(x,z) = \delta(x + z \tan \psi) \{\rho_H[\delta(z - X_h \cos \psi) + \delta(z + X_h \cos \psi)] - \rho_M \delta(z)\}. \quad [10]$$

The form factor corresponding to this transbilayer electron density profile is

$$F_T(\vec{q}) = \rho_M[R_{HM} \cos(q_z X_h \cos \psi - q_x X_h \sin \psi) - 1], \quad [11]$$

where $R_{HM} = 2\rho_H/\rho_M$. We will call this the simple delta function (SDF) model. Following the procedures in ref. 24, we also used a more realistic model, called the 1G hybrid model, that consists of Gaussian functions for the headgroups and the terminal methyl trough and that also allows for differences between the electron density of methylenes and of water. We will call this the simple 1G model. We also considered more complex models that modulated the electron density along the direction perpendicular to $\vec{a}$ in real space in Fig. 1; this is also the direction $\hat{B}$ in reciprocal space, so this modulation strongly affects the $(0,k)$ pure ripple form factors. Our best ripple modulated models (MDF and M1G) had two additional parameters, one to allow for the electron density across the minor side to be different by a ratio f_1 from the electron density across the major side and a second parameter f_2, which is multiplied by δ functions $\delta[(x \pm x_{0/2})]$ to allow for a different electron density near the kink between the major and the minor sides.

Determination of the Phases and the Electron Density Map. Combining Eqs. **6**, **8**, and **11**, the Lorentz-corrected scattering intensity for the (h,k) reflection of the SDF model is

$$I(h,k) = |F(h,k)|^2 = \rho_M^2 \sin^2 \omega_{hk} \left[\frac{k\pi x_0 - \omega_{hk}\lambda_r}{\omega_{hk}\lambda_r(k\pi - \omega_{hk})}\right]^2 \times [R_{HM} \cos(q_z^{hk} X_h \cos \psi - q_x^{hk} X_h \sin \psi) - 1]^2, \quad [12]$$

which contains six independent parameters. Two parameters are related to the ripple profile, namely the ripple amplitude A and the horizontal projection length of the major side of the ripple, x_0. The transbilayer profile contains three parameters, the headgroup to methyl trough electron density ratio (R_{HM}), the monolayer shift angle (ψ), and the headgroup position relative to the center of the bilayer (X_h). The sixth parameter is a common scaling factor for all the $I(h,k)$ peaks. For the simple 1G model, all the transbilayer profile parameters were taken from gel phase data (24) except for the headgroup position X_h. The MDF and M1G models had the two additional parameters, f_1 and f_2, mentioned above. [The parameters λ_r, d, and γ are known from indexing the (h,k) peaks.] Standard nonlinear least squares fitting procedures were employed to obtain unknown parameters by finding the best fit of the intensities given by Eq. **12** to the $|F(h,k)|^2$ reported by Wack and Webb (18). This procedure does not require advance knowledge of any phases. However, once the best values of the parameters in the electron density model are determined, the form factors, and especially the phases, are determined. Using these phases and the amplitudes of the form factors $|F(h,k)|$ from the intensity data (18), an experimental relative electron density map $\rho(\vec{r})$ is obtained using

$$\rho(x,z) = \sum_{h\geq 0} \sum_k F(h,k) \cos(q_x^{hk} x + q_z^{hk} z). \quad [13]$$

RESULTS AND DISCUSSION

The absolute form factors $|F(h,k)|$ reported by Wack and Webb (18) are shown in Table 1 along with two of our many model fits. Our most striking result is that all of our models have the same phases for all the (h,k) reflections displayed in Table 1, except for the pure ripple reflections with $h = 0$. Fig. 2 shows the Fourier map of the electron density using the measured (18) absolute form factors $|F(h,k)|$, omitting the pure ripple reflections $(0,k)$ and our phases, shown in Table 1. Since the $F(0,k)$ are rather small, their inclusion with any phase combination makes rather small differences to the electron density map and negligible differences to the ripple profile.

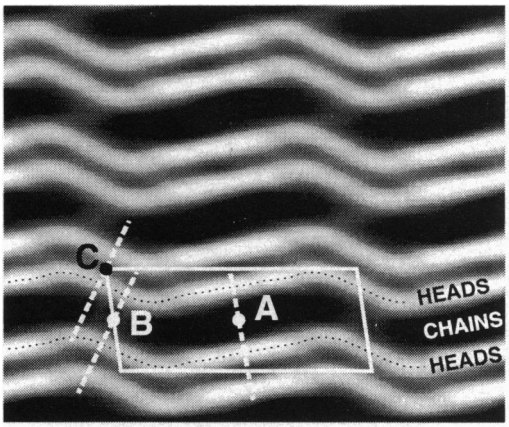

FIG. 2. Electron density map using measured absolute form factors (18) and phases from Table 1, omitting $(0,k)$ reflections. The smallest electron density is pure black and the largest electron density is pure white with a linear gray scale interpolating between. The black dotted lines show two of the loci of maximum electron density. For the electron density along dashed lines A, B, and C, see Fig. 3. The parallelogram shows the unit cell whose width is λ_r, which equals 141.7 Å.

Table 1. Form factors

h	k	$100 \times q$, Å^{-1}	Data* $\|F(h,k)\|$	Model $F(h,k)$ SDF	Model $F(h,k)$ M1G
0	1	4.48	5.3	−1.4	7.9
0	2	8.96	9.7	1.0	−4.6
0	3	13.4	7.8	−0.4	0.9
1	−2	13.0	—	5.0	6.7
1	−1	11.1	60.8	−42.8	−60.4
1	0	10.8	100.0	−96.7	−99.1
1	1	12.3	26.9	38.1	28.5
1	2	15.0	—	−23.6	−11.8
1	3	18.5	7.6	13.9	4.8
1	4	22.3	—	−6.3	−2.4
2	−3	23.8	—	8.6	10.9
2	−2	22.2	15.1	−9.0	−14.1
2	−1	21.5	71.2	−66.9	−71.7
2	0	21.7	39.7	−41.0	−39.9
2	1	22.8	33.9	31.1	30.6
2	2	24.6	22.7	−24.3	−22.8
2	3	27.1	14.2	17.1	15.2
2	4	30.1	7.8	−10.3	−9.1
3	−3	33.3	—	−6.1	−6.0
3	−2	32.5	29.3	22.3	29.0
3	−1	32.2	44.2	42.2	44.5
3	0	32.5	12.0	2.2	0.7
3	1	33.5	—	−11.3	−10.5
3	2	35.0	10.5	14.9	13.9
3	3	37.0	14.9	−15.0	−13.4
3	4	39.4	10.0	12.5	10.8
4	−2	43.0	—	−81.1	−39.2†
4	−1	43.0	—	−63.5	−23.6†
4	0	43.4	—	26.1	10.3†

*From Wack and Webb (18).
†Values are consistent with the densitometer trace shown in figure 4 in ref. 18.

Table 2. Ripple structural quantities

Model	A, Å	x_0, Å	Ψ	X_h, Å	f_1	f_2
SDF	18.6	103	5°	20.1	1.0 (fixed)	0 (fixed)
MDF	20.0	103	9°	20.4	0.7	−2
M1G	19.0	103	9°	19.3	0.6	−1

The ripple profile is shown in Fig. 2 by the dotted lines that are defined as the loci of maximum intensity in the headgroup region. This ripple profile clearly has the basic triangular shape assumed in our modeling, but this result is not tautological because the experimental absolute form factors are employed in Fig. 2. The ripple profile shown in Fig. 2 is in excellent quantitative agreement with the fitted model ripple profiles. The parameters A and x_0 that describe the ripple profile, as well as other parameters in the models, are given in Table 2 for three models. From this we conclude that the ripple amplitude A is about 19 Å and the projection of the major side on the a axis is about 103 Å for the single DMPC sample for which Wack and Webb (18) reported absolute form factors.

To obtain a more quantitative picture of the thickness of the bilayer in various parts of the ripple, electron density profiles (using the experimental $|F(h,k)|$) are plotted in Fig. 3 along the three slices shown by straight dashed lines in Fig. 2 (A, B, and C). Slice A is along the normal of the major side and is centered in the middle of the hydrocarbon region; it indicates that the head–head spacing is 38 Å and the water spacing is 21 Å on the major side. Slice B is along the normal to the minor side and centered in the middle of the hydrocarbon region; it indicates that the bilayer head–head spacing on the minor side is 31 Å. Slice C is along the normal to the minor side, but centered in the water region; it indicates that the water spacing of the minor side is 18 Å. All these spacings are, of course, subject to Fourier truncation errors since the intensity data only include up to three lamellar orders (h = 1–3). Furthermore, no corrections to the form factors have been made to account for fluctuations. For smectic liquid crystals, such corrections are considerably more complex than simple Debye–Waller factors; they are expected to be smaller for the ripple phase than for the fluid L_α phase, and even for this latter phase these corrections change the head–head spacings negligibly (see appendix to ref. 21).

We also performed x-ray experiments on a DMPC sample with almost identical hydration level as the data in ref. 18. The sample was partially dehydrated by a 40% polyvinylpyrrolidone aqueous solution. At 18°C, this sample was in the ripple phase, with a d spacing of 58.1 Å, comparing well with Wack and Webb's value of 57.94 Å. We then took low-angle data at 6°C, at which the sample was clearly in the gel phase with no ripple peaks present. The intensities of five orders $h = 1 - 5$ were recorded, but the electron density profile was reconstructed using the first three orders only so as to form a valid comparison with the ripple phase electron densities that were obtained from experimental data limited to $h = 1 - 3$. The dotted line in Fig. 3*A* shows this comparison. The gel phase profile gives a head–head bilayer thickness of 37.0 Å and a water spacing of 20.8 Å, agreeing well with 37.9 Å and 20.7 Å, respectively, obtained for the ripple phase.

The preceding result strongly suggests that the lipid bilayer along the major side of the ripple is similar to the gel phase bilayer. In contrast, the bilayer along the minor side appears to be thinner, consistent with the working hypothesis that the minor side may be more like the fluid L_α bilayer. A supporting argument for this hypothesis is that the electron density in the headgroup region along the minor side appears to be lower, as it should be for a fluid bilayer with larger area/lipid, than along the major side as shown by the solid curves in Fig. 3*B*. This supporting argument is hardly affected by inclusion of the $F(0,k)$ for the two sets of phases $(-+-)$ and $(+-+)$ for the ripple reflections shown in Table 1. Inclusion makes too little difference to show in Fig. 3*A* for the major side. For the minor side, the $(-+-)$ phase set increases the height of the head groups, but not enough to equal the height for the headgroups on the major side, and not relative to the lower electron density of the chain region. This hypothesis is also consistent with the observation of anisotropic diffusion preferentially along the grooves (26).

Wack and Webb (18) argued that the $(0,k)$ phases are $(+++)$ for k = 1, 2, and 3, although the origin of their unit cell is translated by $b/2$ compared with our unit cell in Fig. 1, so their phases are equivalent to our phase set $(-+-)$, which we obtained from the SDF model as shown in Table 1. However, the small magnitudes of the model $F(0,k)$ motivated us to try the MDF and M1G models that deliberately modulate the total electron density in the direction perpendicular to $\vec{a}$ in Fig. 1. (This direction is also very nearly along the major side since it makes an angle of about 10° with the b axis which is nearly the same as $\gamma - 90°$.) The results for the M1G model given in Table 1, as well as for the MDF model (not shown), show a dramatic improvement in the fit to most of the $F(h,k)$, not just the $F(0,k)$, with a factor of four decrease in the sum of the squares of the residuals. (The crystallographic R value is 0.195 for the SDF model and 0.083 for the M1G model.) It may also be noted that the (0,3) reflection has nearly the same q value as the (1,−2) reflection. Reassignment of the larger part of the value 7.81 for $|F(0,3)|$ in Table 1 to $|F(1,-2)|$ would further improve the fit. However, the set of ripple phases reverses to $(+-+)$ for both the M1G and the MDF model, and this result is unchanged by use of different starting values in the nonlinear least squares fitting program. Therefore, we favor the phases $(+-+)$ for the ripple reflections, although we recognize that none of the models we have considered readily accommodates $|F(0,2)|$ larger than $|F(0,1)|$.

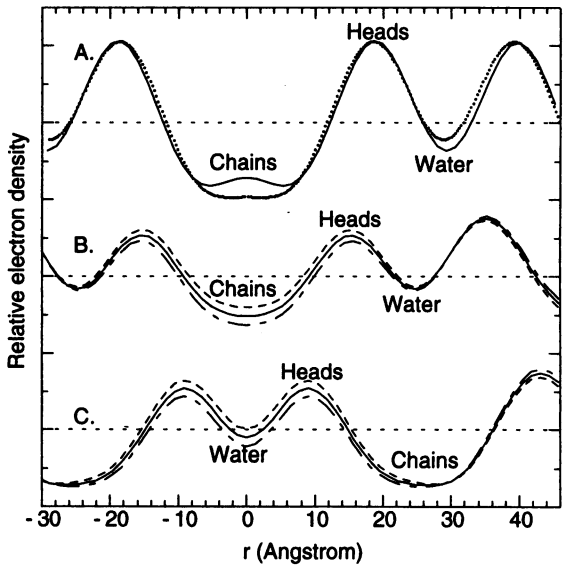

FIG. 3. Solid curves in A, B, and C show electron density along the three dashed lines in Fig. 2 (A, B, and C). The dotted curve in A shows the electron density profile determined for the gel phase. The dashed and dash-dot curves in B and C show the electron density when the $(0,k)$ reflections with phases $(-+-)$ and $(+-+)$, respectively, are added.

Although the phases for the pure ripple $(0,k)$ reflections are not as well-determined by our procedure as the $h \neq 0$ phases, the latter phases, which are very robustly determined using our model method, already determine the ripple profile. Indeed, the effect of different $(0,k)$ phases on the electron density maps is less important than the effect of including the three $h = 4$ reflections shown in Table 1 for the M1G model. Further progress toward understanding the molecular packing of lipids in the ripple phase should employ careful analysis of wide-angle scattering data. This study establishes the framework into which such additional information must be incorporated.

This research was supported by National Institutes of Health Grant GM44976.

1. Doniach, S. (1979) *J. Chem. Phys.* **70,** 4587–4596.
2. Marder, M., Frisch, H. L., Langer, J. S. & McConnell, H. M. (1984) *Proc. Natl. Acad. Sci. USA* **81,** 6559–6561.
3. Hawton, M. H. & Keeler, W. J. (1986) *Phys. Rev. A* **33,** 3333–3340.
4. Carlson, J. M. & Sethna, J. P. (1987) *Phys. Rev. A* **36,** 3359–3374.
5. Goldstein, R. E. & Leibler, S. (1988) *Phys. Rev. Lett.* **61,** 2213–2216.
6. McCullough, W. S. & Scott, H. L. (1990) *Phys. Rev. Lett.* **65,** 931–934.
7. Honda, K. & Kimura, H. (1991) *J. Phys. Soc. Jpn.* **60,** 1212–1215.
8. Lubensky, T. C. & MacKintosh, F. C. (1993) *Phys. Rev. Lett.* **71,** 1565–1568.
9. Tardieu, A., Luzzati, V. & Reman, F. C. (1973) *J. Mol. Biol.* **75,** 711–733.
10. Janiak, M. J., Small, D. M. & Shipley, G. G. (1979) *J. Biol. Chem.* **254,** 6068–6078.
11. Luna, E. J. & McConnell, H. M. (1977) *Biochim. Biophys. Acta* **466,** 381–392.
12. Inoko, Y., Mitsui, T., Ohki, K., Sekiya, T. & Nozawa, Y. (1980) *Phys. Status Solidi A* **61,** 115–121.
13. Copeland, B. R. & McConnell, H. M. (1980) *Biochim. Biophys. Acta* **599,** 95–109.
14. Stamatoff, J. B., Feuer, H. J., Guggenheim, B., Tellez, G. & Yamane, T. (1982) *Biophys. J.* **38,** 217–226.
15. Ruppel, D. & Sackmann, E. (1983) *J. Phys. (Paris)* **44,** 1025–1034.
16. Alecio, M. R., Miller, A. & Watts, A. (1985) *Biochim. Biophys. Acta* **815,** 139–142.
17. Sirota, E. B., Smith, G. S., Safinya, C. R., Plano, F. J. & Clark, N. A. (1988) *Science* **242,** 1406–1409.
18. Wack, D. C. & Webb, W. W. (1989) *Phys. Rev. A* **40,** 2712–2730.
19. Katsaras, J. & Raghunathan, V. A. (1995) *Phys. Rev. Lett.* **74,** 2022–2025.
20. Sun, W., Suter, R. M., Knewtson, M. A., Worthington, C. R., Tristram-Nagle, S., Zhang, R. & Nagle, J. F. (1996) *Phys. Rev. E* **49,** 4665–4676.
21. Nagle, J. F., Zhang, R., Tristram-Nagle, S., Sun, W., Petrache, H. I. & Suter, R. M. (1996) *Biophys. J.* **70,** 1419–1431.
22. Zasadzinski, J. A. N., Schneir, J., Gurley, J., Elings, V. & Hansma, P. K. (1988) *Science* **239,** 1013–1014.
23. Hatta, I., Kato, S. & Takahashi, H. (1993) *Phase Transitions* **45,** 157–184.
24. Wiener, M. C., Suter, R. M. & Nagle, J. F. (1989) *Biophys. J.* **55,** 315–325.
25. Worthington, C., King, G. I. & McIntosh, T. J. (1973) *Biophys. J.* **13,** 480–494.
26. Schneider, M., B., Chan, W. K. & Webb, W. W. (1983) *Biophys. J.* **43,** 157–165.